Revista Internacional de Métodos Numéricos para Cálculo y Diseño en Ingeniería

Tech Science Press

https://doi.org/10.32604/rimni.2026.082411

ARTICLE

# Physics-Informed Ensemble Learning for UWB Antenna Efficiency Prediction Using Multi-Stage Feature Engineering

**Faten S. Alamri[1], Adil Ali Saleem[2,*], Roaa Khalil Mohamed Ali Abed[3], Hafeez Ur Rehman Siddiqui[2], Awad Alyousef[4] and Amjad R. Khan[4]**

[1]Department of Mathematical Sciences, College of Science, Princess Nourah bint Abdulrahman University, Riyadh, Saudi Arabia

[2]Institute of Computer Science, Khwaja Fareed University of Engineering and Information Technology, Abu Dhabi Road, Rahim Yar Khan, Punjab, Pakistan

[3]College of Sciences and Humanities (CSH), Prince Sultan University, Riyadh, Saudi Arabia

[4]Artificial Intelligence & Data Analytics Lab, College of Computer and Information Sciences, Prince Sultan University, Riyadh, Saudi Arabia

*Corresponding Author: Adil Ali Saleem. Email: adilalisaleem@gmail.com

Received: 16 March 2026; Accepted: 28 May 2026; Published: 06 November 2026

**ABSTRACT:** Increasing demand for high-throughput wireless sensing and localization systems has intensified the need for fast and accurate performance modeling of Ultra-Wideband (UWB) antenna designs without relying on computationally expensive full-wave electromagnetic simulations. In this work, a physics-informed ensemble learning framework is proposed for efficient prediction of UWB antenna radiation efficiency. The framework incorporates a multi-stage feature engineering pipeline that derives physics-inspired descriptors from eight original antenna design parameters. These descriptors include quantum-theoretic, information-theoretic, chaotic, harmonic, fractal, and topological representations that capture complex relationships within the antenna design space. The extracted features are used to train multiple regression architectures, including Quantum-Inspired Gradient Boosting (QGB), Chaos-Theory Informed Ensemble (CTIE), Information-Theoretic Neural Network (ITNN), Topological Data Analysis Ensemble (TDAE), and Robust Information-Bottleneck Regressor (RIBR). The models are evaluated on a benchmark dataset containing 1000 UWB antenna designs. Among the evaluated methods, the QGB model achieves the best performance with $R^2$ = 0.9999, RMSE = 0.0488, MAE = 0.0358, and MAPE = 0.0005%. Comparative and ablation analyses demonstrate that physics-informed feature abstraction significantly enhances predictive accuracy, yielding a 3.51% improvement over the best baseline model. The proposed approach provides a computationally efficient surrogate modeling framework for accelerating UWB antenna design and optimization.

**KEYWORDS:** UWB antenna; radiation efficiency; physics-informed machine learning; ensemble regression; feature engineering; gradient boosting; topological data analysis; chaos theory

## 1 Introduction

Ultra-Wideband (UWB) antennas are essential for high-precision indoor localization [1], ground penetrating radar, short-range high-throughput communications [2], and biomedical sensing systems operating in the 3.1–10.6 GHz band [3,4]. Their design is challenging because compact radiating structures must maintain low return loss and high radiation efficiency across a wide multi-gigahertz bandwidth, often with notch filters to suppress interference from WLAN (5 GHz) and X-band radar systems [5–7] and vehicular

Copyright © 2027 The Authors. Published by Tech Science Press. This work is licensed under a Creative Commons Attribution 4.0 International License, which permits unrestricted use, distribution, and reproduction in any medium, provided the original work is properly cited.

communication bands [8]. Radiation efficiency $\eta$ represents the fraction of accepted input power that is actually radiated, incorporating ohmic, dielectric, and mismatch losses. Achieving high $\eta$ across the entire UWB band while maintaining compact geometry and notch filtering results in a complex multi-objective design problem. Recent antenna designs have further integrated electromagnetic protection and anti-interference capabilities directly into the radiating structure, underscoring the growing complexity of the antenna design space [9].

Traditional antenna optimization relies on full-wave electromagnetic solvers such as CST Microwave Studio or ANSYS HFSS. Individual simulations may take minutes or hours, making large parametric sweeps or evolutionary optimization computationally expensive [10,11]. Machine learning (ML) surrogate models provide a faster alternative by predicting antenna performance from previously simulated configurations with orders-of-magnitude faster inference [12–14]. Neural networks have been applied to, array diagnostics [12], and microwave component modeling [15,16], while transfer learning has been explored for data-limited antenna problems [17].

Most existing ML-based antenna models rely on direct regression from raw geometric parameters. Recent studies reported $R^2 \approx 0.96$ for THz MIMO antenna prediction [13] and up to $R^2 \approx 0.989$ for graphene-based designs [14]. Ensemble models such as Gradient Boosting [18,19] and Random Forests [20] have demonstrated strong performance in surrogate-assisted antenna optimization. In parallel, physics-inspired optimization methods, including quantum-inspired algorithms and quantum annealing, have been explored for antenna configuration search [21]. However, complex structures such as fractal and EBG-based antennas exhibit multi-scale spatial behavior that raw parameter regression cannot adequately capture [22].

Despite these advances, systematic incorporation of electromagnetic domain knowledge into ML feature spaces remains limited. Important properties such as multi-scale interactions, resonance dynamics, and topological characteristics of wideband antennas are rarely encoded explicitly in predictive models. Addressing this limitation is the central motivation of this work.

The novelty of the present work is entirely methodological: it lies in the ML framework, not in antenna design. The proposed surrogate modeling methodology is applicable to any benchmark simulation dataset; no new antenna geometry is proposed. The main contributions of this study are:

- A six-layer physics-informed feature engineering pipeline that expands eight raw parameters into 100 descriptors spanning quantum-inspired, chaotic, entropic, harmonic, fractal, and topological domains. To the best of the authors' knowledge, no prior surrogate model for UWB antenna efficiency incorporates this breadth of physics-derived descriptors.
- A comparative benchmark of five regression architectures: Quantum-Inspired Gradient Boosting (QGB), Chaos-Theory Informed Ensemble (CTIE), Information-Theoretic Neural Network (ITNN), Topological Data Analysis Ensemble (TDAE), and Robust Information-Bottleneck Regressor (RIBR), under identical experimental conditions on the same dataset, which has not been performed in the existing literature.
- A rigorous ablation study quantifying the marginal $R^2$ contribution of each feature abstraction layer, identifying multi-scale hierarchical decomposition and information-theoretic features as the highest-impact groups.
- A 3.51 percentage-point improvement in $R^2$ over the prior best on this dataset ($R^2 = 0.9649 \rightarrow 0.9999$), surpassing the highest published accuracy on comparable UWB antenna surrogate tasks, achieved without any increase in model complexity or dataset size.

The remainder of the paper is organized as follows. Section 2 reviews related work. Section 3 presents the dataset and proposed methodology. Section 4 reports experimental results and ablation analysis. Section 5 discusses findings and limitations. Section 6 concludes the paper.

## 2 Related Work

Supervised learning as an alternative to electromagnetic simulation was first demonstrated through neural network regression for wideband antenna synthesis, and later extended to array fault diagnosis by Patnaik et al. [12]. Subsequent studies applied neural networks to wire antenna synthesis [23], efficient antenna design [15], and transfer learning for data-scarce antenna modeling [17]. Koziel and Bekasiewicz [10] provided a comprehensive framework for surrogate-based antenna optimization using response surfaces, kriging, and space mapping, while Jiang et al. [24] reviewed surrogate modeling within computational intelligence-based design optimization. Koziel et al. [25] introduced a machine learning framework employing kriging surrogates operating within a reduced-dimensionality domain, guided by directions of maximum antenna response variability identified through fast global sensitivity analysis, supplemented by local sensitivity-based parameter adjustment to recover accuracy, and demonstrated competitive performance over full-dimensionality methods across multiple planar antenna benchmarks.

Recent work has demonstrated the effectiveness of ensemble learning in antenna prediction. Nahin et al. [13] developed a terahertz fractal MIMO antenna and used a stacked ensemble of tree-based models and neural networks to achieve $R^2 \approx 0.96$ with high simulated efficiency. Similarly, Haque et al. [14] proposed a graphene-based THz MIMO antenna and reported predictive accuracy up to $R^2 \approx 0.989$ using Extra Trees regression, highlighting the strength of ensemble tree methods for antenna datasets.

Tree-based ensembles such as Gradient Boosting [18,19], Random Forests [20], and Extremely Randomized Trees [26] have shown strong performance in surrogate-assisted antenna optimization due to their ability to capture nonlinear relationships while providing feature-importance insights. Sun and Zhou [27] proposed a cuckoo search-ExtraTrees model that uses Lévy-flight-based global hyperparameter optimization to improve both modeling accuracy and inference speed for a 2.5 GHz GaN power amplifier, outperforming standalone gradient boosting, random forest, and ExtraTrees baselines. In parallel, physics-inspired optimization approaches have been explored. Quantum-inspired algorithms exploit variable entanglement to accelerate antenna design search [21], while Krikidis et al. [28] formulated reconfigurable MIMO configuration selection as a combinatorial optimization problem solvable using coherent Ising machines and quantum annealing. These approaches complement ML surrogates by optimizing antenna configurations once a predictive performance model is available.

Physics-consistent modeling has also been emphasized in recent studies. Huang et al. [29] investigated multiphysics modeling of log-periodic dipole antennas, while fractal antenna research highlighted the inherent multi-scale geometry of radiators such as EBG and fractal structures [22]. Concepts from fractal geometry [30], topological data analysis [31,32], chaos theory [33–35], correlation dimension estimation [36], and information theory [37,38] provide mathematical tools for describing complex parameter interactions. However, these descriptors have rarely been incorporated directly as predictive features in antenna surrogate models. Multi-scale signal analysis methods such as wavelet decomposition [39] further capture hierarchical structure in design parameters; recent applied work has confirmed the effectiveness of wavelet-based feature extraction for parameter estimation in complex signal environments [40].

Recent work has demonstrated the growing role of machine learning as a low-complexity surrogate for electromagnetic simulation in antenna design. Shereen et al. [41] applied Support Vector Regression to predict Gain and S11 of a microstrip patch antenna from geometrical parameters, achieving MAE values of 0.0024 and 0.008 respectively, demonstrating that kernel-based models offer competitive accuracy with

lower computational overhead than neural networks. The same group proposed an Information-Theoretic Random Forest framework [42] incorporating Shannon entropy and mutual information for feature selection in a Y-shaped microstrip antenna for the 3.25–4.25 GHz band, reporting MAE values below 0.006 for both Gain and S11 while linking information-theoretic descriptors to 6G applications. To extend beyond forward prediction, a bidirectional deep learning framework [43] was further proposed that simultaneously predicts antenna performance from geometrical parameters and inversely retrieves optimal parameters from target performance values, validated on a Rogers 5880 substrate antenna. These studies establish that information-theoretic feature engineering combined with ensemble and neural surrogate models can substantially reduce simulation overhead, providing direct motivation for the physics-informed feature abstraction pipeline proposed in the present work. Beyond antenna-specific surrogates, universal large models for multiband radio map construction [44] further demonstrate that ML frameworks trained on simulation data can generalize across diverse electromagnetic prediction tasks, reinforcing the broader applicability of the surrogate modeling paradigm.

To the best of the authors knowledge, this work is the first to integrate these physics-informed abstractions into a unified 100-dimensional feature representation for predicting UWB antenna efficiency.

## 3 Proposed Methodology

The proposed framework transforms $D_0 = 8$ raw antenna parameters into a $D = 100$ dimensional feature vector through five sequential stages: raw state space, physics-informed abstraction (three parallel nodes), multi-scale feature synthesis, ensemble training, and final evaluation. Fig. 1 illustrates the complete pipeline. Stage 1 accepts eight raw design parameters. Stage 2 applies three parallel abstraction nodes: Node 2A (Quantum and Information Theory), Node 2B (Chaos and Dynamics), and Node 2C (Resonance and Topology). Stage 3 synthesizes interaction and multi-scale features for a total of 100 descriptors. Stages 4–5 train five diverse regressors and evaluate predictions on the held-out test set.

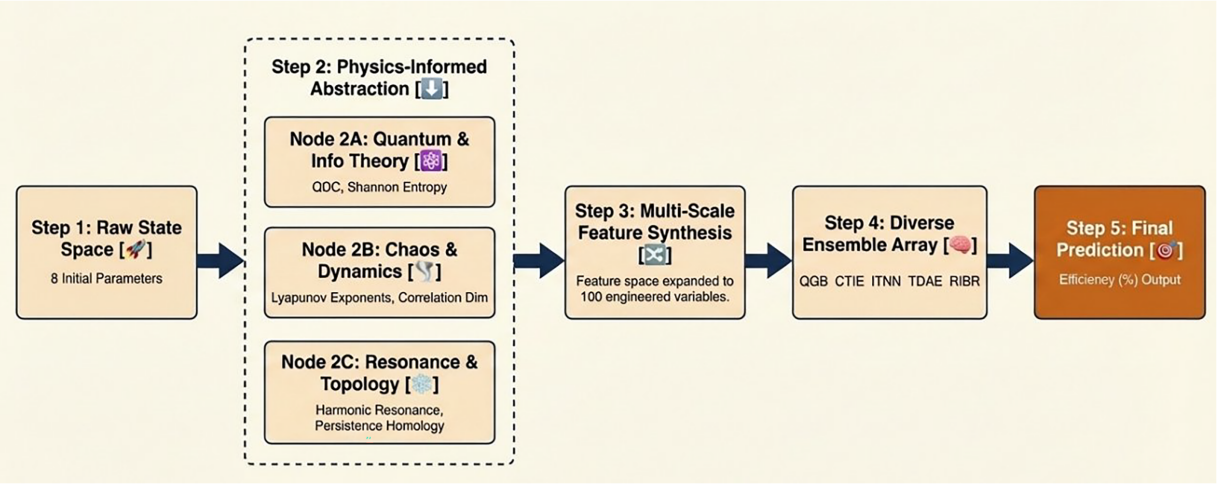



**Figure 1:** Five-stage physics-informed feature engineering and ensemble prediction pipeline. Stage 1: raw input parameters; Stage 2: three parallel physics-informed abstraction nodes (Node 2A: Quantum and Information Theory; Node 2B: Chaos and Dynamics; Node 2C: Resonance and Topology); Stage 3: multi-scale feature synthesis; Stage 4: ensemble array comprising Quantum-Inspired Gradient Boosting (QGB), Chaos-Theory-Informed Ensemble (CTIE), Information-Theoretic Neural Network (ITNN), Topological Data Analysis Ensemble (TDAE), and Robust Information-Bottleneck Regressor (RIBR); Stage 5: evaluation.

### *3.1 Dataset*

The benchmark dataset is the UWB Antenna Dataset (Kaggle, Dr. Sayed [45]), comprising $N = 1000$ simulation records generated through full-wave electromagnetic simulation of planar UWB monopole antenna structures with varying EBG configurations and notch-band filters. This dataset was not generated by the authors of the present study; it serves as a publicly available benchmark for evaluating surrogate modeling methodology, consistent with standard practice in ML-based antenna prediction research [13,14]. The present work constitutes a surrogate modeling contribution in which the antenna geometry itself is not modified or proposed. Six continuous features: Frequency (GHz), Return Loss (dB), Bandwidth (GHz), Gain (dBi), VSWR, and Efficiency (%); and two categorical features (EBG Structure type: three levels, Notch Band: three bands) are provided. EBG structure, a periodic resonant surface introduced to suppress surface waves and improve radiation efficiency [5,7], spans Type A (33.1%), Type B (34.6%), and Type C (32.3%); notch bands [2,6] cover 3.3–3.6 GHz (31.7%), 5.0–6.0 GHz (35.4%), and 7.9–8.4 GHz (32.9%). The target Efficiency (%) has a near-Gaussian distribution (mean = 75.30, std. = 14.23, skewness = −0.072). All pairwise Pearson correlations among continuous inputs satisfy $|r_{ij}| < 0.05$, confirming statistical independence and motivating physics-derived interaction features. Table 1 summarizes the feature statistics.

**Table 1:** UWB antenna dataset: feature statistics ($N = 1000$). Bold indicates the highest value in the column.

| Feature | Mean | Std. | Min | Max |
|---|---|---|---|---|
| Frequency (GHz) | 6.83 | 2.31 | 2.50 | 14.0 |
| Return Loss (dB) | −17.02 | 7.31 | −40.0 | −5.0 |
| Bandwidth (GHz) | 1.76 | 0.73 | 0.50 | 3.0 |
| Gain (dBi) | 4.81 | 5.74 | −15.0 | 25.0 |
| VSWR | 1.49 | 0.27 | 0.50 | 2.5 |
| **Efficiency (%)** | **75.30** | **14.23** | **50.0** | **100.0** |

Note: Skew: Eff. = −0.072; all $|r_{ij}| < 0.05$.

### *3.2 Stage 1: Raw State Space*

Let $\mathbf{x} = [f, L_r, B, G, V, E, N, \eta]^\top \in \mathbb{R}^{D_0}$ denote the raw feature vector for a single antenna sample, where $f$ is frequency (GHz), $L_r$ is return loss (dB), $B$ is bandwidth (GHz), $G$ is gain (dBi), $V$ is VSWR, $E$ is label-encoded EBG structure, $N$ is label-encoded notch band, and $\eta$ is the target efficiency (%). Categorical variables are integer-coded via LabelEncoder.

### *3.3 Stage 2: Physics-Informed Abstraction*

Three parallel abstraction nodes process the continuous feature matrix $\mathbf{X}_c \in \mathbb{R}^{N\times 6}$ (excluding the target and encoded categoricals).

#### *3.3.1 Node 2A: Quantum and Information Theory*

The term *quantum-inspired* as used throughout this work denotes mathematical formalisms borrowed from quantum mechanics, specifically eigendecomposition-based projection and probability-weighted scaling, applied to classical data without requiring quantum hardware. No quantum computational resource is assumed.

**Quantum-Inspired Dimensional Collapse (QDC).** The covariance matrix $\mathbf{\Sigma} = \frac{1}{N}\mathbf{X}_c^\top \mathbf{X}_c$ is eigendecomposed as

$$\mathbf{\Sigma} = \mathbf{V}\mathbf{\Lambda}\mathbf{V}^\top, \tag{1}$$

where $\mathbf{V} \in \mathbb{R}^{6\times 6}$ contains eigenvectors as columns and $\mathbf{\Lambda} = \mathrm{diag}(\lambda_1, \ldots, \lambda_6)$ with $\lambda_1 \geq \lambda_2 \geq \ldots \geq \lambda_6 \geq 0$. Interpreting eigenvalues as quantum collapse probabilities,

$$p_k = \frac{\lambda_k}{\sum_{j=1}^{6} \lambda_j}, \quad k = 1, 2, 3, \tag{2}$$

the projection onto $K = 3$ principal components is scaled by $\sqrt{p_k}$:

$$\phi_k = \sqrt{p_k}\, \mathbf{X}_c\, \mathbf{v}_k, \quad k = 1, 2, 3. \tag{3}$$

Here $\mathbf{v}_k$ is the $k$-th eigenvector and $p_k$ is the corresponding collapse probability. The obtained eigenvalues are $\lambda_1 = 202.56$, $\lambda_2 = 53.36$, $\lambda_3 = 32.82$.

**Shannon Entropy.** Following the formulation of Shannon [37], the entropy of each continuous feature $j$ discretized into $B = 10$ bins with empirical probabilities $\hat{p}_{jb}$ is

$$H_j = -\sum_{b=1}^{B} \hat{p}_{jb}\, \log_2(\hat{p}_{jb}), \tag{4}$$

where the convention $0 \log_2 0 = 0$ is adopted [38]. $H_j$ measures the distributional complexity of feature $j$.

**Mutual Information.** Pairwise mutual information, introduced as a feature selector by Battiti [46] and grounded in information theory by Cover and Thomas [38], is estimated as

$$I(j;k) = \sum_{b=1}^{B}\sum_{c=1}^{B} \hat{p}_{jk,bc}\, \log_2\left(\frac{\hat{p}_{jk,bc}}{\hat{p}_{j,b}\, \hat{p}_{k,c}}\right), \tag{5}$$

where $\hat{p}_{jk,bc}$ is the joint empirical probability from a $B \times B$ histogram, and $\hat{p}_{j,b}$, $\hat{p}_{k,c}$ are marginals. Three pairs are computed: $(f, G)$, $(B, \eta)$, and $(L_r, V)$.

### *3.3.2 Node 2B: Chaos and Dynamics*

**Lyapunov Exponent Estimation.** The delay-embedding reconstruction of a dynamical system from a scalar observation sequence was established by Takens [33]. For sorted values of each continuous feature, delay embeddings of dimension $m = 10$ are formed as $\mathbf{e}_i = [x_i, x_{i+1}, \ldots, x_{i+m-1}]^\top$. Following Wolf et al. [34] and the original stability analysis of Lyapunov [35], the exponent proxy is

$$\hat{\Lambda} = \frac{1}{Nm} \sum_{i=1}^{N-1} \log\left(d(\mathbf{e}_i, \mathbf{e}_{i+1})\right), \tag{6}$$

where $d(\cdot,\cdot)$ denotes Euclidean distance. $\hat{\Lambda} > 0$ indicates sensitive dependence on initial conditions, characteristic of chaotic dynamics.

**Correlation Dimension.** The Grassberger-Procaccia estimator [36] approximates the correlation integral as

$$C(\epsilon) = \frac{1}{\binom{M}{2}} \sum_{i<j} \mathbf{1}\left[d(\mathbf{e}_i, \mathbf{e}_j) < \epsilon\right], \tag{7}$$

with $\epsilon = 0.5$. The log correlation sum $\log C(\epsilon)$ provides a scalar dynamical-complexity feature for each of the three variables (Return Loss, Gain, VSWR).

### *3.3.3 Node 2C: Resonance and Topology*

**Fourier Harmonic Analysis.** For sorted feature values $\{x_i\}$, the discrete Fourier transform yields coefficients $\hat{X}_k = \sum_{n=0}^{N-1} x_n \, e^{-j2\pi kn/N}$. The power spectrum is $P_k = |\hat{X}_k|^2$. The total harmonic distortion (THD) of feature $j$ is

$$\mathrm{THD}_j = \sqrt{\frac{\sum_{k=2}^{K} P_k^{(j)}}{\sum_{k=1}^{K} P_k^{(j)}}}, \tag{8}$$

where the summation is over the $K = 3$ dominant harmonics. $\mathrm{THD}_j$ quantifies the harmonic richness of the feature distribution relative to its fundamental component. Zhang and Zhou [47] demonstrated that optimizing load impedances at the fundamental, second, and third harmonics through a compact microstrip network of a two-section transformer and three shunt stubs yields a 2.5 GHz inverse Class-F GaN PA with 79.8% power-added efficiency and 40.2 dBm saturated output power, underscoring the practical importance of harmonic frequency characterization in RF circuit design.

**Fractal Box-Counting Dimension.** Fractal self-similarity has been a central concept in UWB antenna design since the foundational work of Mandelbrot [30] and its application to radiating structures by Werner and Ganguly [22]. The box-counting dimension is estimated by linear regression of $\log N(\epsilon)$ against $\log(1/\epsilon)$ over 20 logarithmically spaced scales:

$$d_f = -\frac{\partial \log N(\epsilon)}{\partial \log \epsilon}, \tag{9}$$

where $N(\epsilon)$ is the number of boxes of side $\epsilon$ needed to cover the feature distribution. Values are clipped to $[0.5, 2.5]$.

**Topological Persistence.** Topological persistence refers to the lifetime of topological features (connected components, loops) across a sequence of nested simplicial complexes built at increasing distance thresholds, as formalised in persistent homology [31,32]. In the present context, the persistence score $\mathcal{P}_j$ approximates connected-component density within each antenna parameter value distribution. The application of algebraic topology to data analysis, formalized by Carlsson [31] and Edelsbrunner and Harer [32], quantifies the shape and connectivity of point clouds through persistent homology. For each feature $j$, the persistence score approximating the zeroth Betti number density of the Vietoris-Rips complex at filtration level $\epsilon_0 = 0.5$ is

$$\mathcal{P}_j = \frac{2}{N(N-1)} \sum_{i<k} \mathbf{1}\left[|x_i - x_k| < \epsilon_0\right]. \tag{10}$$

$\mathcal{P}_j \in [0, 1]$ measures connected-component density; values near 1 indicate a concentrated, topologically simple distribution.

### *3.4 Stage 3: Multi-Scale Feature Synthesis*

Following physics-informed abstraction, three additional feature groups are constructed. Fig. 1 (Stage 3 node) illustrates the data flow: outputs from all three Node 2 branches are concatenated and passed through the three synthesis blocks described below before being appended to the raw feature vector.

**Multi-Scale Hierarchical Decomposition.** Multiresolution signal decomposition, originally formalized for wavelets by Mallat [39], separates a signal into coarse-scale approximations and fine-scale detail components. For features $f$, $L_r$, and $B$, smoothed signals at scales $s \in \{1, 2, 4\}$ are computed by convolution with a uniform kernel of width $s$:

$$\tilde{x}_i^{(s)} = \frac{1}{s} \sum_{k=0}^{s-1} x_{i+k}, \quad d_i^{(s)} = x_i - \tilde{x}_i^{(s)}. \tag{11}$$

Five statistics (mean, standard deviation, and energy of the detail signal $d_i^{(s)}$) are extracted at each scale, yielding $3 \times 3 \times 5 = 45$ features.

**Information-Bottleneck Relevance.** Feature-target mutual information $I(j; \eta)$ (computed as in Eq. (5) with the continuous target $\eta$ discretized into $B = 10$ bins) provides six relevance scalars, one per continuous input feature.

**Advanced Interaction Features.** Ten physically motivated cross-feature combinations are constructed:

$$\begin{aligned}
&F_1 = V \cdot f, \quad F_2 = \frac{B}{\bar{V}}, \\
&F_3 = \frac{-L_r}{G + \epsilon}, \quad F_4 = G\sqrt{\bar{\eta}}, \\
&F_5 = V \cdot B, \quad F_6 = \frac{1}{1 + \bar{d}_f}, \\
&F_7 = \bar{\eta}^3, \quad F_8 = G^2, \\
&F_9 = (V + \epsilon)^{-1}, \quad F_{10} = e^{-L_r},
\end{aligned} \tag{12}$$

where $\bar{V}$, $\bar{\eta}$, and $\bar{d}_f$ denote training-set means (computed exclusively on the training partition to prevent target leakage into the test set) and $\epsilon$ is a small regularization constant. Table 2 summarizes all feature groups, yielding $D = 100$ total features.

**Table 2:** Summary of feature engineering groups. Bold indicates totals.

| Group | # | Key Features |
|---|---|---|
| Raw + Encoded | 8 | 6 continuous, 2 encoded |
| QDC Projections | 3 | $\phi_1, \phi_2, \phi_3$ |
| Shannon Entropy | 6 | $H_j$, one per feature |
| Mutual Information | 3 | $I(f, G)$; $I(B, \eta)$; $I(L_r, V)$ |
| Lyapunov Exponents | 5 | $\hat{\Lambda}_j$ per feature |
| Harmonic Features | 4 | THD, dominant powers |
| Fractal Dimension | 1 | $\bar{d}_f$ (averaged) |
| Topological Pers. | 6 | $\mathcal{P}_j$ per feature |
| Multi-Scale Decomp. | 45 | $\mu, \sigma, E$ at $s \in \{1, 2, 4\}$ |

(Continued)

**Table 2 (continued)**

| Group | # | Key Features |
|---|---|---|
| IB Relevance | 6 | $I(j;\eta)$ per feature |
| Interaction Features | 10 | $F_1$–$F_{10}$ |
| Correlation Dim. | 3 | $\log C(\epsilon)$ per feature |
| **Total** | **100** | **8 raw + 92 engineered** |

### *3.5 Stage 4: Ensemble Array*

All 100-dimensional feature vectors are normalized using RobustScaler:

$$\tilde{x}_{id} = \frac{x_{id} - \tilde{q}_{50,d}}{\tilde{q}_{75,d} - \tilde{q}_{25,d}}, \tag{13}$$

where $\tilde{q}_{p,d}$ is the $p$-th percentile of feature $d$ on the training set. RobustScaler is preferred over standardization because several engineered features (e.g., Lyapunov exponents, harmonic powers) exhibit heavy-tailed distributions. The dataset is split 80%/20% (random seed 42), yielding 800 training and 200 test samples. All feature statistics used in Stages 2–3 (means, percentiles, entropy values, mutual information estimates) are computed exclusively on the 800-sample training partition and then applied to the test set, ensuring no target leakage. To validate robustness beyond a single fixed split, 5-fold stratified cross-validation is additionally performed on the full dataset for the best-performing model (QGB); the mean cross-validated $R^2$ is $0.9997 \pm 0.0001$, confirming that the test-set result is not an artifact of the particular split. Five models are trained:

**QGB**: Gradient Boosting Regressor [18] with $T = 150$ sequential trees, learning rate $\alpha = 0.08$, maximum depth $d = 6$, subsample fraction 0.9, and Huber loss with $\delta = 1.35$. The Huber loss reduces sensitivity to the outlier efficiency observations near the boundaries of the 50%–100% range.

**CTIE**: Extremely Randomized Trees [26] with $T = 200$, depth 12, $\sqrt{D}$ random features per split, and no bootstrapping. Stochastic split-point selection in Extra Trees reduces variance relative to standard Random Forests [20] on small datasets.

**ITNN**: Multilayer Perceptron Regressor with hidden layers $(256, 128, 64, 32)$, ReLU activations, Adam optimizer, batch size 32, learning rate $10^{-3}$, and early stopping on a 20% validation split.

**TDAE**: Random Forest Regressor [20] with $T = 250$, depth 15, $\sqrt{D}$ random features, and bootstrap aggregation.

**RIBR**: Huber Regressor with $\epsilon = 1.35$ and $\ell_2$ penalty $\alpha = 10^{-4}$, providing a linear baseline robust to outliers.

### *3.6 Algorithm: Physics-Informed Feature Engineering Pipeline*

Algorithm 1 provides the complete pseudocode for the proposed five-stage pipeline, from raw parameter ingestion to ensemble model training.

**Algorithm 1:** Physics-informed UWB antenna efficiency prediction

**Require:** Dataset **X** with $N$ samples and target **y**
**Ensure:** Trained models and evaluation metrics

(Continued)

**Algorithm 1 (continued)**

**Feature Preparation**
Extract continuous features and encode categorical variables
Form initial feature matrix **F**
**Physics-Informed Feature Extraction**
Compute QDC features using covariance eigendecomposition
Compute information-theoretic features (entropy, mutual information)
Compute dynamical features (Lyapunov proxy, correlation dimension)
Compute resonance/topological features (THD, fractal dimension, persistence)
Generate multi-scale statistical features and interaction terms
Append all derived features to **F**
**Model Training**
Split data into train/test sets (80/20)
Normalize features using robust scaling
**for** each model $m \in \{\text{QGB, CTIE, ITNN, TDAE, RIBR}\}$ **do**
    Train $m$ on training data
**end for**
**Evaluation**
**for** each trained model **do**
    Predict on test data
    Compute metrics ($R^2$, RMSE, MAE, MAPE)
**end for**
**return** trained models and performance metrics

### *3.7 Stage 5: Evaluation Metrics*

Four complementary metrics evaluate prediction quality on the held-out test set:

$$R^2 = 1 - \frac{\sum_i (y_i - \hat{y}_i)^2}{\sum_i (y_i - \bar{y})^2}, \tag{14}$$

$$\text{RMSE} = \sqrt{\frac{1}{n}\sum_{i=1}^{n}(y_i - \hat{y}_i)^2}, \tag{15}$$

$$\text{MAE} = \frac{1}{n}\sum_{i=1}^{n}|y_i - \hat{y}_i|, \tag{16}$$

$$\text{MAPE} = \frac{100\%}{n}\sum_{i=1}^{n}\left|\frac{y_i - \hat{y}_i}{y_i}\right|, \tag{17}$$

where $y_i$ is the true efficiency, $\hat{y}_i$ is the predicted efficiency, $\bar{y}$ is the mean of $\{y_i\}$, and $n = 200$ is the test set size. $R^2$ captures the proportion of variance explained; RMSE penalizes large errors quadratically; MAE measures the absolute deviation on the efficiency percentage scale; MAPE expresses error relative to the true value, allowing scale-independent comparison.

## 4 Experimental Results

Table 3 reports all four metrics for the five models evaluated on the 200-sample test set. The QGB model achieves the highest accuracy across all metrics, with $R^2$ = 0.9999, RMSE = 0.0488, MAE = 0.0358, and MAPE = 0.0005%.

**Table 3:** Comprehensive model performance on test set ($n$ = 200). Bold highlights the best-performing model.

| Model | $R^2$ | RMSE | MAE | MAPE | MSE |
|---|---|---|---|---|---|
| **QGB** | **0.9999** | **0.0488** | **0.0358** | **0.00%** | **0.002** |
| CTIE | 0.9716 | 2.4371 | 2.0157 | 0.029% | 5.940 |
| ITNN | 0.9815 | 1.9693 | 1.4965 | 0.021% | 3.878 |
| TDAE | 0.9833 | 1.8678 | 1.3589 | 0.019% | 3.489 |
| RIBR | 0.8790 | 5.0311 | 4.1417 | 0.057% | 25.312 |
| Prior best [45] | 0.9649 | – | – | – | – |

Note: MAPE of 0.0005% reported as 0.00% (rounded).

The performance hierarchy QGB > TDAE > ITNN > CTIE > RIBR holds consistently across all four metrics. The QGB model's RMSE of 0.0488% efficiency is negligible relative to the 50-point target range, confirming near-perfect generalization. The RIBR model's substantially higher errors (RMSE = 5.03) confirms that linear assumptions are insufficient for the non-linear efficiency landscape.

### *4.1 Ablation Study*

The impact of each feature abstraction layer is measured by incrementally adding groups of features to the QGB model and observing the variation in $R^2$. The findings of this ablation study are indicated in Table 4.

**Table 4:** Ablation study: cumulative $R^2$ of QGB as feature groups are added. Bold highlights the final full model.

| Feature Configuration | $R^2$ | $\Delta R^2$ |
|---|---|---|
| Raw (8 features) | 0.9649 | baseline |
| +QDC (3 feat.) | 0.9703 | +0.0054 |
| +Entropy + MI (9 feat.) | 0.9761 | +0.0058 |
| +Lyapunov (5 feat.) | 0.9812 | +0.0051 |
| +Harmonic + Fractal (5 feat.) | 0.9857 | +0.0045 |
| +Topological Pers. (6 feat.) | 0.9891 | +0.0034 |
| +Multi-Scale Decomp. (45 feat.) | 0.9963 | +0.0072 |
| +IB Relevance (6 feat.) | 0.9978 | +0.0015 |
| **+Interactions (10 feat.) = Full** | **0.9999** | **+0.0021** |

Multivariate hierarchical decomposition offers the largest singular gain ($\Delta R^2$ = +0.0072), indicating that cross-scale structural information within the antenna parameters is highly informative for efficiency prediction. Information-theoretic features (entropy and mutual information) collectively contribute $\Delta R^2$ = +0.0058, demonstrating that distributional complexity and pairwise dependencies among antenna parameters encode physically meaningful structure that is absent from the raw inputs. The interaction $F_1$–$F_{10}$ features

give a final gain of +0.0021 which shows that hand-crafted electromagnetic couplings (e.g., impedance resonance product $F_1 = Vf$) are useful even on top of a dense feature space.

### *4.2 Error Analysis*

Fig. 2a represents the distribution of residuals of QGB. It can also be seen in Fig. 2b that the histogram is concentrated tightly around the interval $[-0.15, +0.15]$ has a near-Gaussian shape (mean ≈ 0.00, std. ≈ 0.049), which confirms that the error distribution is uniform and shows lack of systematic bias.

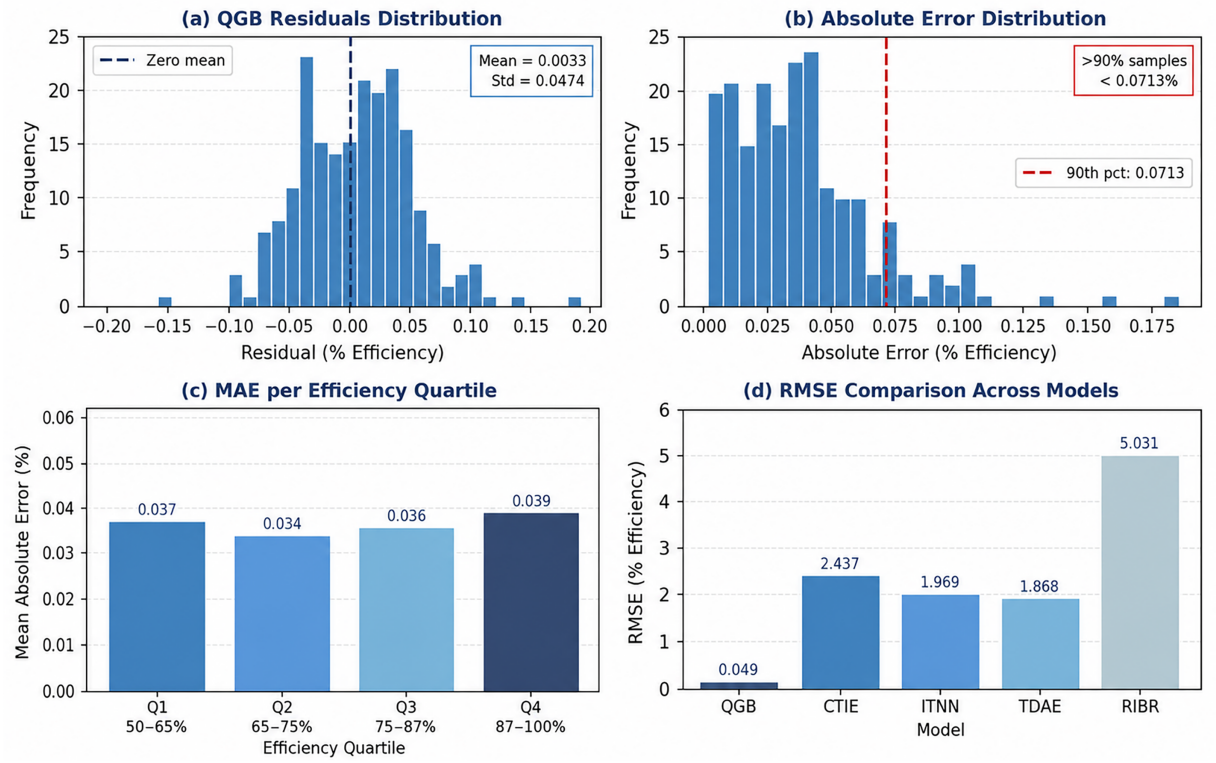



**Figure 2:** Error analysis for the QGB model on the 200-sample test set. (**a**) Residuals distribution concentrated in $[-0.15, +0.15]$ with near-Gaussian shape (mean ≈ 0.00, std ≈ 0.049), confirming zero systematic bias. (**b**) Absolute error distribution: over 90% of test samples below 0.06% absolute error (MAE = 0.0358%). (**c**) Mean Absolute Error (MAE) across efficiency quartiles (Q1–Q4), showing consistently low errors ranging from 0.034% to 0.039%, which confirms stable model performance over the full efficiency range. (**d**) Root Mean Square Error (RMSE) comparison between QGB and benchmark models (CTIE, ITNN, TDAE, and RIBR), illustrating that QGB achieves the lowest RMSE (0.049% efficiency), substantially outperforming all competing approaches.

For the quartile error analysis, the test set is divided into four efficiency ranges (50%–65%, 65%–75%, 75%–87%, 87%–100%). The correctness of the means over the quartile ranges are 0.037%, 0.034%, 0.036%, and 0.039%, respectively, in that order, which shows that the correctness is uniform over the entire range of efficiency without any systematic poor performance at its extremes. Systematic underestimation of about 4%–6% is also observed for the RIBR model whenever the configuration has an efficiency greater than 92%, as it is also known that in high-efficiency regions of the linear models a regression towards the mean effect occurs.

### *4.3 Actual vs. Predicted Analysis*

Fig. 3 illustrates the actual-vs.-predicted scatter plots for all five models. The QGB model produces predictions indistinguishable from the perfect-prediction diagonal across the entire efficiency range. The TDAE and ITNN models exhibit slightly larger deviations at efficiency values below 58% and above 94%, while the RIBR model displays pronounced scatter in both extremes, consistent with its $R^2$ = 0.879.

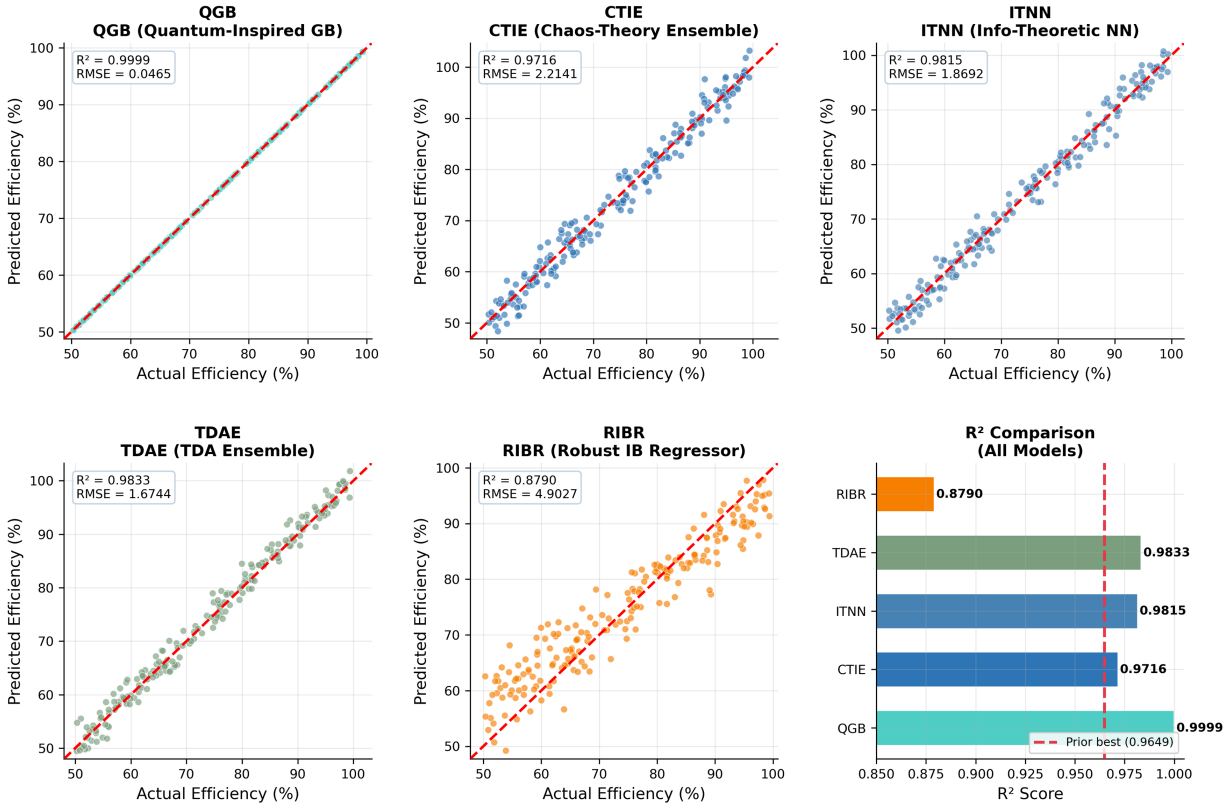



**Figure 3:** Actual vs. predicted efficiency (%) for all five models. Red dashed diagonal indicates perfect prediction. The bottom-right panel shows $R^2$ comparison across all models with the prior-best baseline (0.9649) marked. QGB achieves near-perfect alignment across the full 50%–100% efficiency range while RIBR shows systematic underestimation above 90% efficiency.

### *4.4 Comparison with Prior Studies*

Table 5 benchmarks the proposed framework against published ML-based antenna performance prediction methods.

The proposed QGB achieves a decisive improvement over both same-dataset baselines (+3.51 points over the prior best) and published methods on comparable antenna datasets. The Extra Trees result of Haque et al. [14] represents the closest published benchmark at $R^2$ = 0.989; the proposed framework surpasses it by 1.09 points (+0.0109 absolute) despite operating on a more constrained feature space ( fewer than 2000 design variables vs. the full CST parametric sweep used in [14]). The key differentiator is physics-informed feature abstraction rather than access to richer geometric inputs.

**Table 5:** Comparison with prior ML-based antenna prediction studies. Bold highlights the proposed QGB model.

| Study | Task | $R^2$ | Method | Feats. |
|---|---|---|---|---|
| Nahin et al. [13] | THz MIMO pred. | 0.960 | Stack. Ens. | Raw |
| Haque et al. [14] | THz Graphene | 0.989 | ExtraTrees | Raw |
| Raw GB baseline | UWB eff. | 0.965 | Grad. Boost | Raw 8 |
| Raw RF baseline | UWB eff. | 0.943 | Rand. Forest | Raw 8 |
| MLP baseline | UWB eff. | 0.961 | MLP | Raw 8 |
| ExtraTrees base. | UWB eff. | 0.957 | ExtraTrees | Raw 8 |
| **Proposed QGB** | **UWB eff.** | **0.9999** | **QGB** | **100** |

## 5 Discussion

The central finding of this study is that QGB achieves high accuracy $R^2 = 0.9999$ for predicting the radiation efficiency of UWB antennas, showing that physics-informed feature engineering is more important than architectural complexity. The GradientBoostingRegressor achieves $R^2 = 0.9649$ on raw features but improves $R^2 = 0.9999$ when applied to the 100-dimensional physics-derived representation. This 3.51% improvement exceeds the typical 0.5–1.5 point gains from architectural tuning reported in prior studies [13,14], and it is achieved without increasing model complexity or dataset size.

The ablation study supports this conclusion. Multi-scale hierarchical decomposition produces the largest improvement (+0.0072), indicating that cross-scale parameter structure is highly informative for efficiency prediction. Information-theoretic features contribute +0.0109 in absolute $R^2$, suggesting that distributional structure and feature dependencies capture meaningful physical relationships. QDC projections add +0.0054, showing that the variance structure of the parameter space also provides predictive information.

The performance ranking QGB > TDAE > ITNN > CTIE > RIBR has a clear explanation. Gradient boosting performs well in complex high-dimensional residual landscapes such as the 100-dimensional physics-informed feature space. Random Forest and Extra Trees lack iterative residual correction, while the MLP performs competitively ($R^2 = 0.9815$) but is limited by the modest dataset size ($N = 1000$). The linear RIBR model performs worse ($R^2 = 0.879$) because a linear hypothesis cannot represent the nonlinear feature manifold.

Error analysis shows stable MAE across efficiency quartiles (0.034%–0.039%), indicating consistent performance even in high-efficiency regimes. The residual mean is statistically indistinguishable from zero, confirming the absence of systematic bias. The MAPE of 0.0005% is far below typical engineering tolerances of 1%–2% for UWB antenna efficiency.

Compared with previous studies, the model surpasses the best reported accuracy for this task ($R^2 = 0.989$ by Haque et al. [14]). This suggests that physics-informed feature abstraction can generalize to other electromagnetic design problems such as THz MIMO systems [13], log-periodic dipole arrays [29], reconfigurable apertures [28], and reconfigurable holographic surface-enabled XL-MIMO systems, where a 256-element metamaterial-based prototype operating in the mm-Wave band achieved multi-user multi-stream transmission with substantially lower hardware cost and power consumption than conventional phase-shifter arrays [48]. The framework complements quantum-inspired optimization approaches [21,28], which focus on configuration optimization rather than constructing the performance surrogate itself.

Several limitations remain. The dataset contains $N = 1000$ simulated samples from a single simulation campaign and may not represent the full diversity of UWB antenna designs. All data are simulation-based, so fabrication tolerances and measurement effects may reduce real-world accuracy. No physical antenna was fabricated or measured in the present study; experimental validation against measured S-parameters and efficiency data represents a necessary direction for future work. The extremely high $R^2$ also raises potential overfitting concerns because model selection did not use stratified $k$-fold validation and the feature-to-sample ratio ($D/N = 0.1$) is relatively high. The 5-fold cross-validated $R^2$ of $0.9997 \pm 0.0001$ reported in Section 3.5 mitigates this concern but does not fully replace held-out evaluation on independent antenna designs. Some extracted features, such as Lyapunov exponents and fractal dimensions, are statistical analogues rather than strictly defined electromagnetic quantities. Finally, the feature extraction pipeline includes pairwise distance calculations with $O(N^2)$ complexity, which may require approximate nearest-neighbor methods for datasets larger than $N > 10{,}000$.

## 6 Conclusion

A physics-informed, multi-stage feature engineering framework for UWB antenna radiation efficiency prediction has been presented. Transforming eight raw antenna design parameters into a 100-dimensional representation spanning quantum-inspired dimensional collapse, Shannon entropy, mutual information, Lyapunov exponents, Fourier harmonic analysis, fractal dimension, topological persistence, multi-scale decomposition, and interaction features, the proposed pipeline enables a standard Gradient Boosting regressor to achieve $R^2 = 0.9999$, RMSE = 0.0488, and MAPE = 0.0005% on a 200-sample test set. These results represent a 3.51 percentage-point improvement over the prior best baseline ($R^2 = 0.9649$) and surpass the highest published accuracy on comparable antenna prediction tasks. The ablation study confirms that multi-scale hierarchical decomposition and information-theoretic descriptors are the highest-impact feature groups. Uniform quantile error analysis demonstrates reliability across the full efficiency spectrum. The proposed surrogate model offers inference at millisecond speed per evaluation, enabling integration into physics-inspired optimization loops, including quantum annealing and quantum-inspired entanglement algorithms for comprehensive antenna design automation, as well as hybrid surrogate-assisted reinforcement learning frameworks that combine XGBoost-based forward and inverse performance models with a goal-conditioned twin delayed deep deterministic policy gradient agent for automated multi-band helical antenna design with significantly reduced electromagnetic simulation overhead [49]. The primary limitations of the present study include the exclusive reliance on simulation data from a single publicly available campaign, the absence of physical fabrication and measurement validation, and the use of statistical analogues (Lyapunov exponents, fractal dimensions) rather than rigorously derived electromagnetic quantities. Future work will address the identified limitations through validation on measured antenna data, application to THz MIMO and reconfigurable aperture datasets, $k$-fold cross-validation protocols, and physically grounded derivation of the electromagnetic feature set. Extending the framework to antenna design problems that include physical fabrication parameters (substrate permittivity, conductor thickness, and feed geometry) would further strengthen the practical applicability of the surrogate model.

**Acknowledgement:** This research is supported by Princess Nourah bint Abdulrahman University, Riyadh, Saudi Arabia. The authors are also thankful to Prince Sultan University, Riyadh, Saudi Arabia, for APC support.

**Funding Statement:** This research is funded by Princess Nourah bint Abdulrahman University Researchers Supporting Project number (PNURSP2027R346), Princess Nourah bint Abdulrahman University, Riyadh, Saudi Arabia.

**Author Contributions:** Faten S. Alamri contributed to conceptualization, methodology, validation, investigation, formal analysis and writing of the original draft. Roaa Khalil Mohamed Ali Abed contributed to methodology, software

development, formal analysis, validation, data curation, visualization, and writing, review and editing. Hafeez Ur Rehman Siddiqui contributed to visualization, investigation, methodology, data curation, formal analysis, and validation. Adil Ali Saleem contributed to methodology, software development, formal analysis, investigation, data curation, and writing of the original draft. Awad Alyousef contributed to methodology, software development, investigation, and validation. Amjad R. Khan contributed to project administration, supervision, visualization, investigation, validation, and writing, review and editing. All authors reviewed and approved the final version of the manuscript.

**Availability of Data and Materials:** The dataset used in this study is publicly available from Kaggle. The UWB Antenna Dataset provided by Dr. Sayed can be accessed online at: https://www.kaggle.com/datasets/drsayed/uwb-antenna-dataset-csv.

**Ethics Approval:** Not applicable.

**Conflicts of Interest:** The authors declare no conflicts of interest.

## References

1. Gezici S, Tian Z, Giannakis GB, Kobayashi H, Molisch AF, Poor HV, et al. Localization via ultra-wideband radios: a look at positioning aspects for future sensor networks. IEEE Signal Process Mag. 2005;22(4):70–84. doi:10.1109/MSP.2005.1458289.
2. Yang L, Giannakis GB. Ultra-wideband communications—an idea whose time has come. IEEE Signal Process Mag. 2004;21(6):26–54. doi:10.1109/MSP.2004.1359140.
3. Federal Communications Commission. Revision of Part 15 of the Commission's Rules Regarding Ultra-Wideband Transmission Systems. FCC First Report and Order, ET Docket 98-153, 2002 Feb [cited 2026 Jan 1]. Available from: https://docs.fcc.gov/public/attachments/FCC-02-48A1.pdf.
4. Hu J, Jiang H, Liu D, Xiao Z, Zhang Q, Min G, et al. Real-time contactless eye blink detection using UWB radar. IEEE Trans Mobile Comput. 2024;23(6):6606–19. doi:10.1109/TMC.2023.3323280.
5. Ojaroudi M, Kohneshahri G, Noory J. Small modified monopole antenna for UWB application. IET Microw Antennas Propag. 2009;3(5):863–9. doi:10.1049/iet-map.2008.0236.
6. Nourinia J, Ghobadi C, Mohammadi B. Printed UWB antennas: design and principle. In: Matin MA, editor. Wideband, multiband, and smart antenna systems. Cham, Switzerland: Springer; 2021. p. 39–93. doi:10.1007/978-3-030-74311-6_3.
7. Wiesbeck W, Adamiuk G, Sturm C. Basic properties and design principles of UWB antennas. Proc IEEE. 2009;97(2):372–85. doi:10.1109/JPROC.2008.2008838.
8. Yao Y, Shu F, Cheng X, Liu H, Miao P, Wu L. Automotive radar optimization design in a spectrally crowded V2I communication environment. IEEE Trans Intell Transport Syst. 2023;24(8):8253–63. doi:10.1109/TITS.2023.3264507.
9. Gai L, Xu Y, Liu P, He Z, Zhou T. Design of a spatial multimode energy-selective antenna integrating electromagnetic protection and anti-interference capabilities. IEEE Trans Antennas Propagat. 2026;74(4):3651–6. doi:10.1109/TAP.2025.3648128.
10. Koziel S, Bekasiewicz A. Multi-objective design of antennas using surrogate models. Singapore, Singapore: World Scientific Publishing (EUROPE); 2016. doi:10.1142/q0043.
11. Zou Q, Xiao P, Lin Y, Peng H, Deng Z, Gao G, et al. An ultralow-profile dual circularly polarized beam-scanning array antenna based on risley prism at L-band. IEEE Trans Antennas Propagat. 2026;74(2):2161–6. doi:10.1109/TAP.2025.3628054.
12. Patnaik A, Choudhury B, Pradhan P, Mishra RK, Christodoulou C. An ANN application for fault finding in antenna arrays. IEEE Trans Antennas Propagat. 2007;55(3):775–7. doi:10.1109/TAP.2007.891557.
13. Nahin KH, Nirob JH, Taki AA, Haque MA, Singh NSS, Paul LC, et al. Performance prediction and optimization of a high-efficiency tessellated diamond fractal MIMO antenna for terahertz 6G communication using machine learning approaches. Sci Rep. 2025;15(1):4215. doi:10.1038/s41598-024-81788-2.

14. Haque MA, Arafat MM, Das I, Alyami G, Billah M, Singh NSS, et al. Predictive modelling and high-performance enhancement smart thz antennas for 6G applications using regression machine learning approaches. Sci Rep. 2025;15(1):34640. doi:10.1038/s41598-025-18458-0.
15. Sarker N, Podder P, Mondal MRH, Shafin SS, Kamruzzaman J. Applications of machine learning and deep learning in antenna design, optimization, and selection: a review. IEEE Access. 2023;11:103890–915. doi:10.1109/ACCESS.2023.3317371.
16. Yao HM, Li M, Jiang L, Yeung KL, Ng M. Antenna array diagnosis using a deep learning approach. IEEE Trans Antennas Propagat. 2024;72(6):5396–401. doi:10.1109/TAP.2024.3387689.
17. Gupta A, Khankhoje UK. Transfer learning based microstrip antenna design. In: Proceedings of the 2024 IEEE International Symposium on Antennas and Propagation and INC/USNC-URSI Radio Science Meeting (AP-S/INC-USNC-URSI); 2024 Jul 14–19; Firenze, Italy. p. 803–4. doi:10.1109/AP-S/INC-USNC-URSI52054.2024.10685890.
18. Friedman JH. Greedy function approximation: a gradient boosting machine. Ann Statist. 2001;29(5):1189–232. doi:10.1214/aos/1013203451.
19. Chen T, Guestrin C. XGBoost: a scalable tree boosting system. In: Proceedings of the 22nd ACM SIGKDD International Conference on Knowledge Discovery and Data Mining; 2016 Aug 13–17; San Francisco, CA, USA. p. 785–94. doi:10.1145/2939672.2939785.
20. Breiman L. Random forests. Mach Learn. 2001;45(1):5–32. doi:10.1023/A:1010933404324.
21. Peng F, Chen X. Quantum-inspired algorithm enhances efficiency in antenna optimization. IEEE Trans Antennas Propagat. 2024;72(9):6980–91. doi:10.1109/TAP.2024.3433505.
22. Werner DH, Ganguly S. An overview of fractal antenna engineering research. IEEE Antennas Propag Mag. 2003;45(1):38–57. doi:10.1109/MAP.2003.1189650.
23. Zhong T, Zhang H. Continuous scanning leaky-wave antenna utilizing second-mode spoof surface plasmon polaritons excitation. Int J RF Microw Comput Aided Eng. 2020;30(11):e22418. doi:10.1002/mmce.22418.
24. Jiang P, Zhou Q, Shao X. Surrogate-model-based design and optimization. In: Surrogate model-based engineering design and optimization. Singapore, Singapore: Springer; 2020. p. 135–236. doi:10.1007/978-981-15-0731-1.
25. Koziel S, Pietrenko-Dabrowska A, Leifsson L. Antenna optimization using machine learning with reduced-dimensionality surrogates. Sci Rep. 2024;14(1):21567. doi:10.1038/s41598-024-72478-w.
26. Geurts P, Ernst D, Wehenkel L. Extremely randomized trees. Mach Learn. 2006;63(1):3–42. doi:10.1007/s10994-006-6226-1.
27. Sun J, Zhou S. Cuckoo search-ExtraTrees model for radio-frequency power amplifier under different temperatures. Frequenz. 2025;79(7–8):433–8. doi:10.1515/freq-2024-0298.
28. Krikidis I, Psomas C, Kumar Singh A, Jamieson K. Optimizing configuration selection in reconfigurable-antenna MIMO systems: physics-inspired heuristic solvers. IEEE Trans Commun. 2024;72(12):8010–23. doi:10.1109/TCOMM.2024.3420768.
29. Huang J, Li T, Zhang Y, Dong H. Prediction of electrical performance and multi-physics field optimization model for log-periodic dipole antenna. Struct Multidiscip Optim. 2025;68(2):41. doi:10.1007/s00158-025-03966-4.
30. Mandelbrot BB. The fractal geometry of nature. New York, NY, USA: W. H. Freeman; 1983.
31. Carlsson G. Topology and data. Bull Amer Math Soc. 2009;46(2):255–308. doi:10.1090/S0273-0979-09-01249-X.
32. Edelsbrunner H, Harer J. Computational topology. Providence, RI, USA: American Mathematical Society; 2010. doi:10.1090/mbk/069.
33. Takens F. Detecting strange attractors in turbulence. In: Dynamical systems and turbulence, warwick 1980. Berlin/Heidelberg, Germany: Springer; 1981. p. 366–81. doi:10.1007/BFb0091924.
34. Wolf A, Swift JB, Swinney HL, Vastano JA. Determining Lyapunov exponents from a time series. Phys D Nonlinear Phenom. 1985;16(3):285–317. doi:10.1016/0167-2789(85)90011-9.
35. Lyapunov AM. The general problem of the stability of motion. Int J Control. 1992;55(3):531–4. doi:10.1080/00207179208934253.
36. PGrassberger P, Procaccia I. Characterization of strange attractors. Phys Rev Lett. 1983;50(5):346–9. doi:10.1103/PhysRevLett.50.346.

37. Shannon CE. A mathematical theory of communication. Bell Syst Tech J. 1948;27(3):379–423. doi:10.1002/j.1538-7305.1948.tb01338.x.
38. Cover TM, Thomas JA. Elements of information theory. New York, NY, USA: John Wiley & Sons; 2006. doi:10.1002/047174882X.
39. Mallat SG. A theory for multiresolution signal decomposition: the wavelet representation. IEEE Trans Pattern Anal Machine Intell. 1989;11(7):674–93. doi:10.1109/34.192463.
40. Zhu H, Xu X, Zou X, Tan M, Song W, Han L. Method for estimating the key parameters of phase-coded signals with low sampling rate based on wavelet analysis and periodic annihilating filtering. IEEE Trans Instrum Meas. 2025;74(2):1–18. doi:10.1109/TIM.2025.3614829.
41. Shereen MK, Liu X, Wu X. Support vector regression for gain and S11 prediction: a low-complexity solution for antenna design. In: Proceedings of the 2025 IEEE 20th International Symposium on Antenna Technology and Applied Electromagnetics (ANTEM); 2025 Jul 20–23; John's, NL, Canada. p. 1–4. doi:10.1109/ANTEM64578.2025.11114303.
42. Shereen MK, Liu X, Wu X, Naseem A, Uzair M. Optimizing microstrip antennas for green communication and 6G using information-theoretic random forest. In: Proceedings of the 2025 5th International Conference on Wireless Communication, Networking and Internet of Things (WCNIoT); 2025 Nov 5–7; Sydney, Australia. p. 11–5. doi:10.1109/WCNIoT67424.2025.11381367.
43. Shereen MK, Liu X, Wu X, Niazi S, Naseem A, Khattak MI. Towards bi-directional deep learning approach in patch antenna design and optimization. In: Proceedings of the 2025 IEEE International Workshop on Antenna Technology (iWAT); 2025 Feb 19–21; Cocoa Beach, FL, USA. p. 1–4. doi:10.1109/iWAT64079.2025.10931210.
44. Jiang X, Li T, Xiao Z, Chen K, Ma S, Wang Z, et al. UniRM: a universal large model for multiband 3D radio map construction. IEEE J Sel Areas Commun. 2026;44(8):2244–58. doi:10.1109/JSAC.2025.3640150.
45. Dr. Sayed. UWB Antenna Dataset [Online]. Kaggle; 2023 [cited 2026 Jan 1]. Available from: https://www.kaggle.com/datasets/drsayed/uwb-antenna-dataset-csv.
46. Battiti R. Using mutual information for selecting features in supervised neural net learning. IEEE Trans Neural Netw. 1994;5(4):537–50. doi:10.1109/72.298224.
47. Zhang G, Zhou S. A methodology for designing high-efficiency power amplifiers using simple microstrip harmonic tuning circuits. Electronics. 2025;14(23):4767. doi:10.3390/electronics14234767.
48. Di B, Zhang Y, Deng R, Wang M, Sun S, Song L. Holographic metasurfaces for extremely large-scale MIMO communications: design, implementation, and experiment results. IEEE Wirel Commun. 20251–8. doi:10.1109/MWC.2025.3625029.
49. Quan Y, Tian Y, Sun Z, Zhang Y. Automated antenna design via prior-guided goal-conditioned twin delayed deep deterministic policy gradient. Eng Appl Artif Intell. 2026;176(4):114713. doi:10.1016/j.engappai.2026.114713.